ESTIMATES OF OIL SPILL DISPERSION EXTENT IN THE NEARSHORE ALASKAN BEAUFORT SEA BASED ON IN-SITU OCEANOGRAPHIC MEASUREMENTS

Seth L. Danielson

and

Thomas J. Weingartner

Institute of Marine Science
University of Alaska
Fairbanks, AK
99775-7220

21 May 2007

Prepared for the

Alaska Department of Environmental Conservation

ADEC Division of Spill Prevention and Response
555 Cordova St.
Anchorage, AK
99516-2617

This page intentionally left blank.

Abstract

This report describes analyses designed to estimate the distance and direction an oceanic oil spill could travel during each of the two primary circulation regimes found in the near-shore Beaufort Sea: 1) under landfast ice during winter and 2) in open water or partial ice cover during summer. This information will aid the Alaska Department of Environmental Conservation (ADEC) in oil spill response planning.

Year-round measurements were made at six separate nearshore sites over the course of five calendar years, for a total of 14 instrument-years of data. Many measurements were made in relatively close proximity to oil production activities. Analyses are based on the progressive vector diagram, which follows the path that a hypothetical particle would take if released at the mooring site and then is subsequently freely advected by the ocean currents. The analyses comprise our best estimate of particle displacements over short time periods based upon in-situ oceanographic data from the North Slope. Results allow us to place approximate bounds on the distance an oil spill could traverse during each of the primary circulation regimes.

Primary findings include the following. 1) Over the 2-day to 12-day time frames considered here, displacement of an oil spill will be relatively small during the landfast ice period (tens of kilometers) and relatively large during the open water and drifting ice period (hundreds of kilometers). 2) Advection in the summer is highly dependent upon the wind speed and direction. 3) In both seasons, transport of oil in the alongshore (east-west) direction is greater than transport in the cross-shore (north-south) direction. In aggregate, the findings suggest that the average oil slick leading edge would move about 2 km per day in the winter and 15 km per day in the summer. In rare cases, oil can move 6 km per day in the winter and 60 km per day in the summer. Frictional coupling, trapping of oil within ice pores, topographic steering, and other interaction between the oil, water, ice and sediment could degrade the accuracy of these results.

ADEC can improve its oil spill response preparedness for this region by undertaking additional measures. Analysis and synthesis of existing datasets and model output would help place the results of this report into a broader spatial context and would help define the limits of applicability. Much basic oceanographic research is still needed to describe and understand the nature and causes of circulation over the Beaufort shelf. Implementing an oceanic monitoring program for the purposes of knowing ocean conditions before and during an oil spill would allow spill responders to act in a more informed fashion and make better decisions. New technologies can be employed to meaningfully aid in an actual oil spill response effort.

This page intentionally left blank.

Table of Contents

This page intentionally left blank.

Acknowledgements

We thank the Minerals Management Service for providing the funding to carry out the observations (award numbers 1435-01-03-CT-74221 and 1435-01-00-CA-31083) and BP for providing logistical support. David Leech designed, fabricated, deployed and recovered the moorings. He was ably assisted by Steve Okkonen, Bill Williams, Jeremy Kasper, and Kevin Taylor. Thank you all.

This page intentionally left blank.

1. Introduction

Arctic continental shelves are shallow zones (<100 m) between the land and the deep Arctic Ocean (> 3000 m) that are strongly influenced by the wind, river discharge, freeze/thaw cycles, ice and topography. The Alaskan Beaufort shelf extends approximately 600 km alongshore and 80 km in the cross-shore direction (**Figure 1**). This shelf has few large-scale relief features over the central portion, but is bisected by Barrow Canyon to the west and the Mackenzie Canyon to the east. Since the 1970s, oil production activities have expanded from Prudhoe Bay both eastward and westward and more recently in the offshore direction.

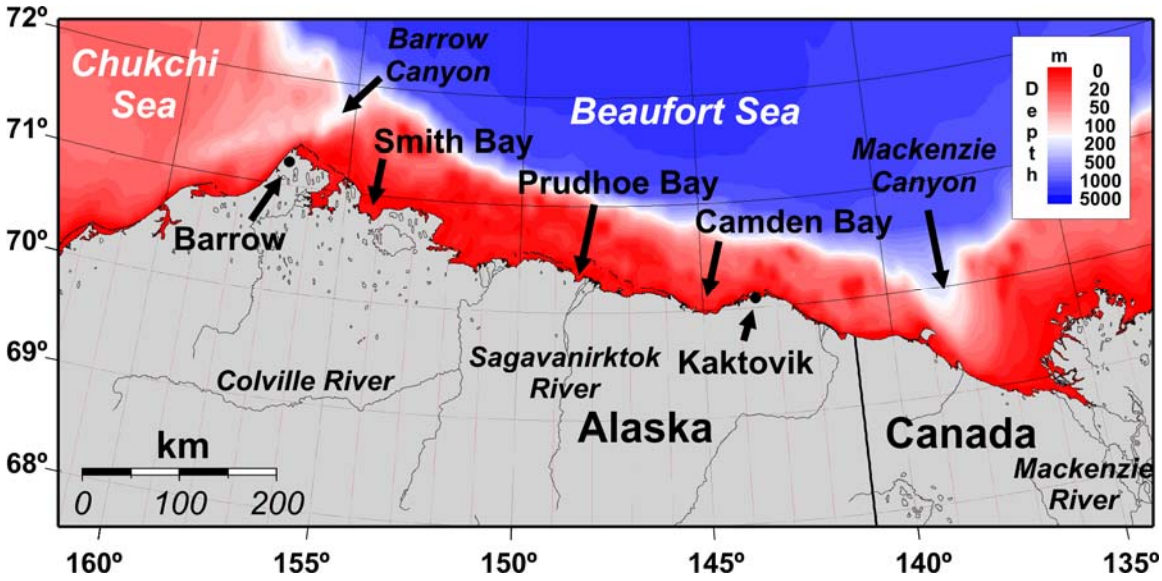

Figure 1. Regional map showing the Beaufort Sea bathymetry, the location of Smith, Prudhoe and Camden Bays, select rivers, and the coastal villages of Barrow and Kaktovik.

This report describes analyses designed to estimate the distance and direction an oceanic oil spill could travel during each of the two primary circulation regimes found in the near-shore Beaufort Sea: 1) under landfast ice during winter and 2) in open water or partial ice cover during summer. This information will aid ADEC in oil spill response planning for the Beaufort Sea area. Related documents are available on the ADEC Division of Spill Prevention and Response Industry Preparedness Program web page: http://www.dec.state.ak.us/spar/ipp/nscharter.htm.

We analyze velocity data to estimate the distance that an oil spill could traverse along Alaska's North Slope. The methods employed herein are only one of a variety of methods that resource managers might use in the development oil spill contingency plans. These in-situ measurements offer the following advantages: 1) the observational time series extend over multiple years and all seasons, 2) the measurements reflect actual oceanographic conditions and 3) some measurements were made in relatively close proximity to oil production activities.

In contrast, oil spill trajectory models are limited by spatial resolution (often tens of kilometers), the bathymetry is not everywhere well known, they require parameterization of features smaller than the model's spatial resolution (e.g., ice keels, ridges, cracks and pores are not resolved), and models require parameterization of processes that can not be analytically described (e.g., ice rafting and ridging, frictional coupling between oil, ice, water, suspended sediment and the seafloor). Many oil spill trajectory models do not account for the presence of ice or buoyancy (fresh water) driven circulation (including the NOAA GNOME model that ADEC employs for oil spill trajectory forecasts). As we will see, both ice and fresh water play an important role for the circulation of the Beaufort Sea shelf.

Previous current meter measurements in the Beaufort Sea were primarily made during the Outer Continental Shelf Environmental Assessment Program (OCSEAP). These measurements often had limited deployment durations and were located in offshore waters, but the spatial coverage is more extensive than at the sites given in this report [Aagaard, 1981 and Aagaard et al, 1989]. Further information about the Beaufort Sea physical oceanography, literature references, and reports can be accessed at the following web page: http://www.ims.uaf.edu/beaufort/.

In Section 2, we briefly describe relevant aspects of the Beaufort Sea physical oceanography. The observational dataset and the instrumentation employed are described in Section 3. In Section 4 we present the analysis techniques and discussion of their limitations. Section 5 contains results and specific caveats about this data in relation to the Beaufort Sea environmental conditions. Section 6 describes the modern suite of oceanographic instrumentation and methods that could be employed to facilitate an oil spill response. The technology described could be useful to ADEC during the process of evaluating the best available technology (BAT) to respond to oil spills. Section 7 presents recommendations to ADEC to enhance our ability to quantify and/or predict the fate of oil spills in the Beaufort Sea. Section 8 provides additional discussion of results and final conclusions.

2. Oceanographic Background

Ocean currents along Alaska's North Slope inner shelf behave in two distinctly differing modes over the course of one year [Weingartner et al, 2005]. During the *landfast ice period* when the nearshore ice field is immobile and mechanically fixed to the shore, current magnitudes are generally small (**Figure 2d**) and are uncorrelated with the wind forcing. During the *open water and freely drifting ice period* the currents are more vigorous and are primarily wind-driven, as shown in **Figure 2d** and **Figure 3**. The analysis employed herein is based upon these two time periods.

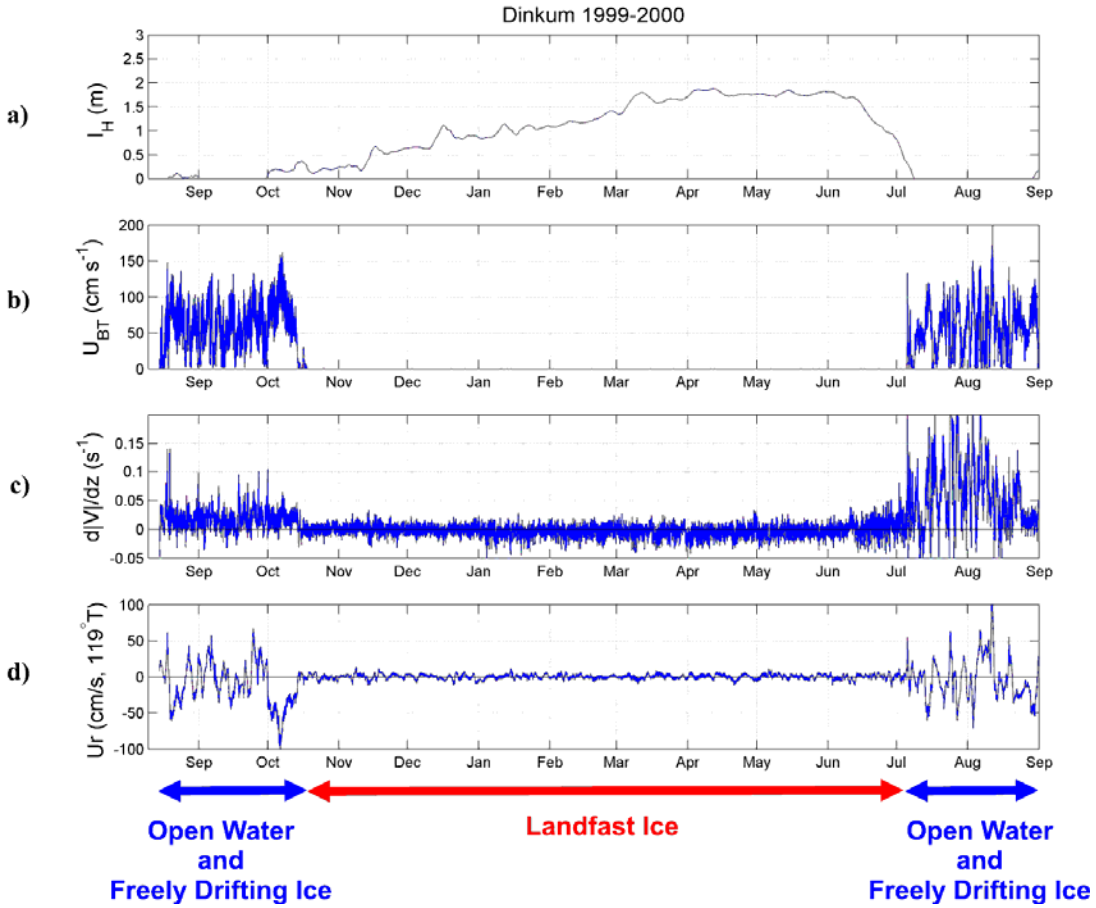

Figure 2. Yearlong time series plots of **a)** ice thickness, **b)** surface/ice velocity, **c)** vertical shear and **d)** along-shore water velocity at the Dinkum site between August 1999 and 2000. The landfast ice season is determined by the period of zero ice velocity. Positive velocity values are directed to the east. Note stronger currents and stronger current shear during the summer months (reproduced from Weingartner et al., 2005).

Pack ice is sea ice that is relatively mobile. Even in the presence of 100% ice cover, pack ice responds to both winds and ocean currents by deforming or by moving in response to the forces applied by the atmosphere and ocean. The wind stress transfers energy through the pack ice to the ocean and thus is able to drive ocean currents beneath pack ice. First year (young) pack ice is typically less than 2 m thick, while multi-year pack

ice can grow to thickness greater than 6 m. *Landfast ice* is sea ice that is rigidly attached to the coast and/or the sea floor and acts as an immobile lid upon the ocean. Therefore, wind stress is not transferred to the ocean through landfast ice. Landfast ice forms every winter and does not typically exceed 2-3 m in thickness. However, ridged or piled up pack or landfast ice can become grounded in water depths of 20m or more. Strong wind or ocean currents can cause ice pile-up and ridging. A transition zone between the nearshore landfast ice and the offshore pack ice commonly is an area of intense seafloor reworking, bulldozing and gouging by deep ice keels [Barnes, et. al, 1984]. Gouging of ice keels on the seafloor presents considerable risk to instrumentation, hence the need for our short mooring configuration (described below). The edge of the landfast is often near the 20 m isobath, but recent work has shown considerable variability in its extent [Mahoney et al, 2005].

The landfast ice period generally extends from mid October or early November to early July; the remaining months comprise the open water or ice in free drift season. There is often a one or more week transition period between the two regimes while the landfast ice sets up in the fall and during breakup in the spring. For shorthand, we also refer to the landfast ice period as the "winter" season and the open water/free ice drift period as the "summer" season.

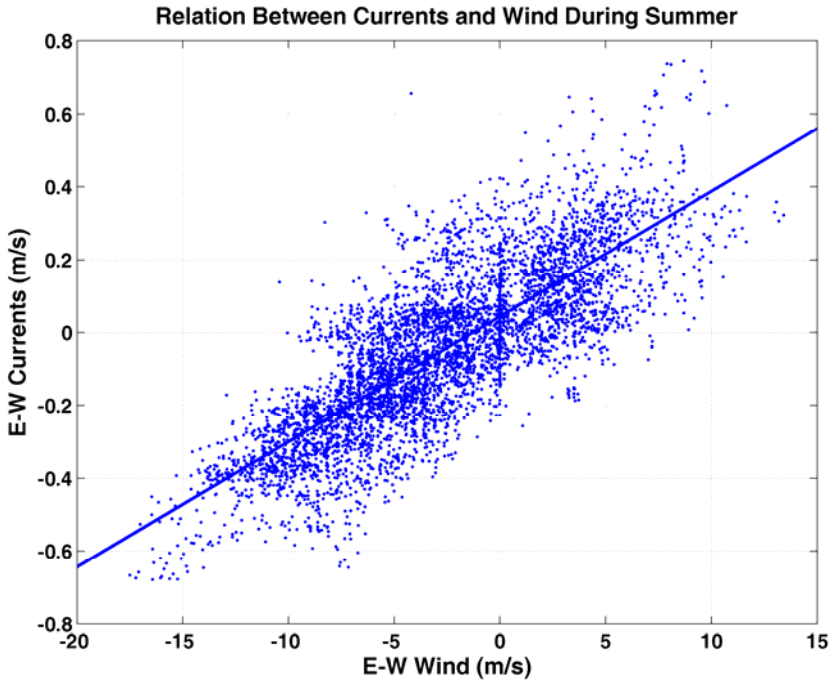

Figure 3. Summertime nearshore zonal currents vs. zonal winds. The plot shows the tight coupling between the two parameters. The wind data account for 67% of the variance of the current data (correlation coefficient r = 0.82 with the winds leading the currents in time by six hours). The blue line is the best fit straight line to the data. Positive wind and current values represent flow to the east, negative to the west. Current data are taken here from the Dinkum site; wind data are from the Deadhorse airport, National Weather Service station PASC. There is not a significant relationship between the meridional (N-S) winds and currents.

The annual cycles of ice growth, river discharge and summer melt together with the waxing and waning of storm systems combine to give the shelf its characteristic flow patterns described above. These effects all combine to also influence the vertical distribution of currents, as shown below.

Arctic shelves are inundated with fresh water during the spring freshet: 90% of the annual river discharge can occur in the ~2 week span surrounding the peak discharge, which occurs in the presence of landfast ice, usually in June. The fresh river water flows out below and above the landfast ice and above the cold (-1.8º C) and salty shelf water. Shelf water is denser than river water and will preferentially lie below the fresh surface layer. Without wind energy available to mix the fresh surface plume with the lower salty ocean water (because of the landfast ice), the uppermost portion remains fresh and can support large currents whose speed and direction is largely independent of the currents lower in the water column. In summer, the greatest shear between the surface and mid-depth waters are observed in July (**Figure 2c**), consistent with this being the period of greatest stratification due to river discharge and ice melt and before fall storms homogenize the water column by wind mixing.

In the winter, the flow is influenced by frictional stress at the seabed and beneath the ice. The current and shear magnitudes are small, however, varying by only 1 or 2 cm/s over the course of the water column (**Figure 4a**). In the summer, after the landfast ice is gone, the winds force the water at the surface. This surface forcing, in addition to the stratification provided by the surface ice melt and river discharge creates velocity shear distributed through the water column (**Figure 4b**). For this reason, it is important to measure currents as close to the top of the water column as possible when considering an oil slick floating on and being advected by water.

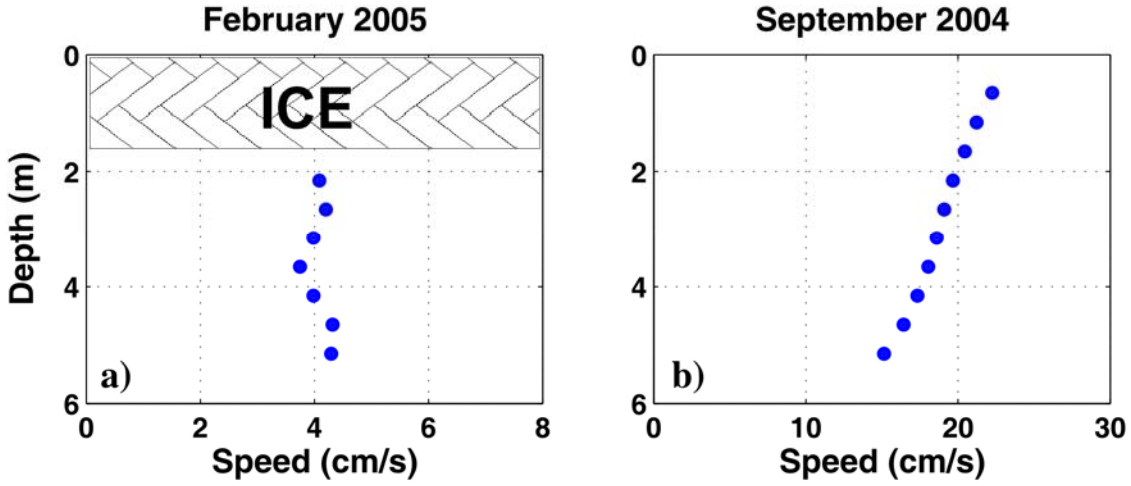

Figure 4. Vertical distribution of the mean current magnitude at the Dinkum site during the months of February 2005 (left) and September 2004 (right). Note the difference in horizontal scales. Summer shear is greater than in the winter, due to the combined effects of open water wind forcing in conjunction with stratification. The seafloor was at 6.7 m depth.

3. Measurements

The analyses presented here are based on measurements supported by the Minerals Management Service (MMS) between 1999-2002 (Phase I) and 2004-2007 (Phase II). A summary of results from the Phase I deployments is given in Weingartner et al [2005]. Measurements were made at a total of six sites, four within 40 km of Prudhoe Bay, one 220 km (120 nautical miles) to the west in Smith Bay and one 130 km (70 nautical miles) to the east in Camden Bay (**Figure 5)**. As of September 2006, we have recovered nearly 14 instrument-years worth of velocity data from the deployments (**Table 1**). The Dinkum, Argo and McClure sites are all situated between barrier islands and the shoreline, whereas the Reindeer, Smith Bay and Camden Bay sites are located seaward of all barrier islands.

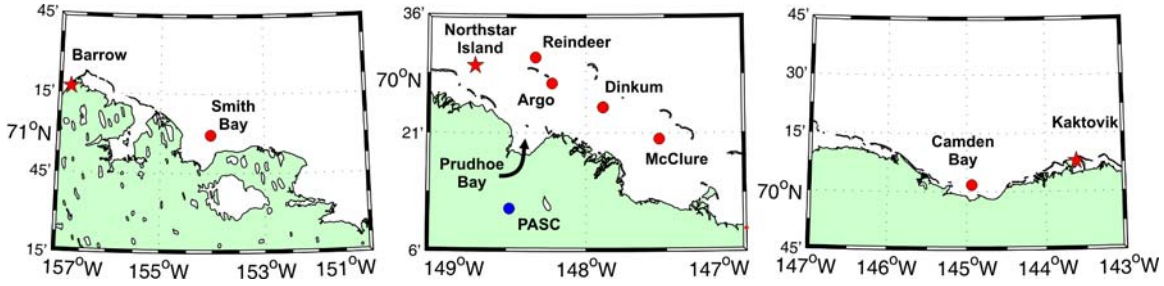

Figure 5. Maps showing locations of the Smith Bay mooring (left), the Prudhoe Bay moorings (center) and the Camden Bay mooring (right). Northstar Island is located with a red star in the center figure. Northstar Island is an oil production island constructed in 2000 and 2001. The McClure mooring lies within the undeveloped Liberty field. PASC is the location of the Deadhorse airport weather station.

Water current speed and direction measurements are made with 1200 KHz and 600 KHz Teledyne RD Instruments Acoustic Doppler Current Profilers (ADCPs). ADCPs measure water velocity by computing the Doppler shift imposed on high frequency sound waves that are reflected off of ambient sound scatterers drifting freely in the water column, such as passively drifting zooplankton [Gordon, 1996]. The scatterers are advected by the ocean currents and on average move with the same velocity as the water itself. The ADCPs are mounted close to the bottom, looking upward toward the surface (**Figure 6**). Since the speed of sound in water is known, by time gating the reflected acoustic signals returning from the scatterers, the instrument is able to create a profile through the water column of the current speed and direction at evenly spaced "bins" from about 1m above the instrument to within about 1m of the surface. The set of all bins for one sample period is called a measurement "ensemble". For each final measurement within an ensemble, the ADCP makes approximately 200 individual samples at each bin depth, which are then averaged into a single value at each bin depth for each ensemble time period, resulting in a final accuracy of approximately 0.5 cm/s.

The ADCPs are programmed to collect 2-3 ensembles per hour for the course of one calendar year, in ½ meter bins spaced from approximately 1.5 meters above the bottom to about 1 meter below the surface. We consider here only data from the bin closest to the surface with good data. In practice, the absolute closest bin to the surface is contaminated by waves and acoustic side-lobe reflections, so we use data from the second-closest bin.

Mooring Site	Latitude (ºN)	Longitude (ºW)	Years with good ADCP Data	Bottom Depth (m)
Argo	70º 27.18’	148º 12.72’	1999-2000 2000-2001 2001-2002	8.4
Camden Bay	70º 01.69’	144º 56.59’	2004-2005 2005-2006	8.6
Dinkum	70º 24.35’	147º 53.66’	1999-2000 2000-2001 2001-2002 2004-2005 2005-2006	6.8
McClure	70º 20.20’	147º 32.70’	1999-2000 2000-2001	6.7
Reindeer	70º 30.54’	148º 19.21’	2001-2002	12.7
Smith Bay	70º 59.28’	154º 02.00’	2004-2005	9.8

Table 1. Summary of deployment site names, locations, periods of water velocity data collection, and nominal total water depth. All deployments and recoveries took place in the months of August or September. The Reindeer, Smith Bay and Camden Bay deployments sites are located outside of all barrier islands; the other sites are between barrier islands and the shore.

Figure 6. An example of the oceanographic mooring employed for our measurements. The top of the ADCP is approximately 0.5 m above the frame bottom. The orange pop-up buoy facilitates recovery at the end of the deployment. The fat white pressure case on the left contains extra battery power for the ADCP; the thin white pressure case on the right is an instrument that measures pressure, temperature, salinity and transmissivity.

As the ice grows thicker through the winter, the depth of this near-surface bin deepens through the water column and then ascends again as the ice melts in late spring (**Figure 2a**).

In addition to the current speed and direction measurements, the motion of any hard reflecting surface is also measured by the ADCPs. In the summer, wave action and inhomogeneity of the ice field results in a noisy surface signal; in the winter the ice bottom provides a stable reflection surface with a clear signal for ice motion tracking. Thus, we define the landfast ice period as between the start and end of consistently zero ice velocity measurements in the fall and late spring (**Figure 2b**).

4. Analysis

The approach we employ herein is based on the Progressive Vector Diagram (PVD) analysis. The PVD computation involves integrating the path that a hypothetical particle would follow if released at the mooring site and then is subsequently carried by the ocean currents. For the measurement interval Δt (=1200 to 1800 seconds), analysis period $T=n\cdot\Delta t$ (T = 2, 4, 8 and 12 days), zonal flow $u(t)$ and meridional flow $v(t)$, the particle's x- and y- (eastward and northward) displacements at the end of the integration period are given by (1):

$$X(n) = \sum_{t=1}^{n} \Delta t \cdot u(t)$$
$$Y(n) = \sum_{t=1}^{n} \Delta t \cdot v(t) \qquad (1)$$

An example PVD is given in **Figure 7.** Measurements were taken every 20-30 minutes, depending on the deployment site and deployment year, and the PVD integrations are run for 2, 4, 8 and 12 days. Particles are initialized daily at midnight, so the number of particles given on the plots below is the same as the total number of days of observations at the mooring site. For integrations that cross the boundary between the two seasons, the results are assigned to the open water and free drift season. Currents measured during mid-winter landfast ice breakout events (rare at most of our sites) are considered to be within the landfast ice season.

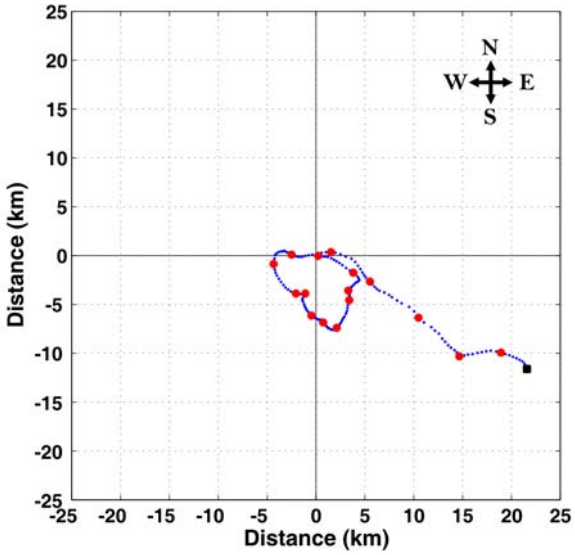

Figure 7. An example PVD from the Argo site initialized at midnight of August 15, 1999 at the center point (0, 0). Measurements were made every 30 minutes. The particle position is plotted at every time step with the blue dots, red dots are plotted every 6 hours and the final location is plotted in black. The integration spans a total of 4 days. After making a clockwise loop that took about 64 hours, the particle drifted to the south-east for the final 32 hours. The ending location is described by the integration endpoints $X(n)=21.6$ and $Y(n)=-11.6$. In this example, the maximum distance attained by the particle (measured from the start location) is the same as the final distance.

PVD analysis assumes that the flow field is spatially homogenous. For analyses in which the particle does not stray far from the starting location, this assumption is generally valid. Our previous reports [e.g., Weingartner, 2005] indicate that during the landfast ice period, currents are typically coherent over spatial scales of at least 30km. During the free ice drift and open water period, currents are coherent over distances greater than 100 km. The integral time scale (de-correlation time scale) of oceanic motion is approximately 2-5 days in the winter and 3-6 days in the summer. Thus, these overlapping analyses are not fully independent samples, resulting in fewer degrees of freedom than the total number of PVD iterations run. Additionally, it means that the longer 8 and 12 day integrations amount to 2 – 6 independent measurements. Nonetheless, this method will result in a statistically similar distribution of particles as a smaller ensemble of fully independent samples. While there are many ways to construct the PVDs, we believe that starting the integration only once per day is a conservative approach that provides a good balance between keeping the integrations somewhat independent yet providing a reasonably clear picture of the likely particle distributions over the course of both seasons.

Other sources of error that can cause the PVD integration to diverge from real world water-borne drifting oil include the following:

1. Frictional coupling manifested within in the near-surface ADCP blanking area between any of: the oceanic flow, the wind, landfast or pack ice, and oil
2. Seafloor, coastal, or under-ice topographic steering
3. Flow convergences and divergences
4. Inhomogeneities in the ocean forcing fields (wind, river discharge, etc)
5. Trapping of oil within ice cracks and pores
6. Oil spill containment devices

The magnitude of all of these error sources is variable in both space and time and can not be resolved with our dataset. Thus, rather than imposing artificial constraints to approximate these error sources, we have kept the analysis straightforward for ease of interpretation. For example, Cox and Schultz [1980] describe laboratory experiments that define velocity magnitude threshold values required to transport oil under smooth ice and ice with small-scale roughness once the oil has reached an equilibrium thickness. We neglect such threshold values in this study because the large-scale under-ice topography may have a larger effect on actual oil spill dispersal and the under-ice topography is not well known. Moreover, oil may spread over considerable distances before it has attained its equilibrium thickness.

5. Results

Table 2 and **Table 3** presented below contain seasonally partitioned summary statistics for the analyses. **Figures 8 – 12** are summary plots for the 4-day analysis at the Dinkum site, the mooring site with the largest data set. See **Appendices A-F** for complete sets of figures corresponding to all six mooring deployment locations and for analyses that span 2, 4, 8 and 12 day periods for both the landfast ice and open water seasons.

The figures captions associated with **Figures 8-12** apply to the corresponding figures in the appendices but are given there in abbreviated form.

Caveats and comments to help guide interpretation:

Some details of the oceanographic data and the background environmental conditions require further comment. The following list describes some practical limits of the combined dataset and the PVD analyses when applied to oil spill trajectories.

a. In an oil spill under the ice, oil can be absorbed within the ice matrix. After breakup or a landfast ice breakout event, landfast ice is mobile so the location that the ice subsequently melts and oil re-enters the water may be far removed from the location where the oil was entrained.

b. The topographic landscape of the underside ice surface is not well known. Keels and other features could act to channel oil and funnel it a great distance or block oil from moving in a particular direction. Keels and other topography can change an oil spill's spatial extent even in the absence of currents. A greater area may be required to achieve the equilibrium oil slick thickness due to ice keels extending down in the water column below an oil slick. Conversely, concave topographic features may act to trap oil in thicker pools.

c. Oceanographic conditions presented here are all from shallow water sites located close to shore and under landfast ice in the winter. The PVD analysis endpoint locations were primarily found to be within this same domain. We do not expect that our results apply at locations in deeper water and closer to the landfast ice edge or under the drifting pack ice beyond the landfast ice edge. The seaward extent of landfast ice and its variability is described by Mahoney, et al. [2005]. An oil spill in offshore waters may impact the nearshore domain (and vice-versa), but we can not address these scenarios with the present data set.

d. Circulation offshore from major rivers will likely behave differently than at the sites in this study, including regions near the Colville, Kuparuk and Canning rivers. In particular, the period following maximum river discharge is a critical time period. The fresh river plume could disperse oil in the offshore direction, as opposed to the normally along shore flow observed at our mooring sites.

e. Although the ADCP measurements are taken from the uppermost bin with good data, the ADCP measurements are contaminated in the bin actually closest to the sea surface

or the ice bottom. Thus, our measurements located slightly below where surface oil would float. During the spring river freshet, the currents in this thin topmost layer could be quite strong and possibly different than in the closest good bin to the surface. During the winter, there is little if any stratification and the currents are typically more vertically uniform.

f. At the sites occupied in this study, landfast ice breakout events (detachment of a portion of the landfast ice canopy) are unusual. Landfast ice breakout events may be more common at other locations. We expect higher under-ice currents and farther particle displacements at and near breakout events. The Smith Bay mooring was deployed beneath and sampled during one landfast ice breakout event.

g. River discharge and summer storms can create high levels of turbidity (suspended sediment) in the water column. Sediment entrained into oil plumes will change its density and may affect where in the water column the oil will be found. Moreover, sediments are incorporated into landfast ice during its fall formation. Oil covered sediments within the ice matrix might subsequently be released after breakup and melt back into the water. This may occur far from the location in which incorporation occurred.

Description of Summary Statistics Tables:

Table 2 presents summary statistics for the ***open water and freely drifting ice period***; **Table 3** presents summary statistics for the ***landfast ice period.***

- All distances are given in km, measured from the mooring site. All integrations began at position (0, 0) and were initialized daily at midnight.
- The ***Analysis Length*** indicates the PVD integration period in days.
- ***N*** is the number of PVD integrations.
- The ***Maximum Displacement*** columns refer to the particle's farthest displacement attained within the integration period.
- The ***Final Displacement*** columns refer to the particle position at the end of the integration period (the position locations plotted in **Figures 8 and 9**).
- The ***Greatest Maximum and Final Displacement*** columns describe the single farthest displacement observed within each set of integrations given in the *Maximum* and *Final Displacement* columns.
- The ***Mean Final Zonal and Meridional Displacement*** (east-west/north-south) columns describe the central point of all ending particle locations. In these columns, negative values indicate westerly and southerly displacement; positive values indicate easterly and northerly displacement. The winter values are small and negative, indicating that nearly as many particles travel east (north) as those that travel west (south), but with a slight bias to the west and to the south at most sites. Summer values are more commonly biased to the west and to the north.
- The total number of seasonal observations and weighted mean values (based on number of observations per site) are given in red.
- The largest mean maximum, greatest maximum and mean final displacements for each integration period are highlighted in yellow.

Table 2: Open Water and Freely Drifting Ice Period Summary Statistics

Mooring	Analysis Length (days)	N	Mean Maximum Displacement (km)	Maximum Displacement Standard Deviation (km)	Greatest Maximum Displacement (km)	Mean Final Displacement (km)	Mean Final Distance Standard Deviation (km)	Greatest Final Displacement (km)	Mean Final Zonal Displacement (km)	Mean Final Meridional Displacement (km)
Argo	2	318	33.8	25.4	140.3	32.5	26.3	140.3	-8.3	2.3
Dinkum	2	541	37.9	26.9	134.4	36.2	28	134.4	-8.2	7.4
McClure	2	232	29.8	22.6	109.7	28.6	23.4	109.7	-0.3	4.4
Reindeer	2	90	44.5	31.9	114.6	43.5	32.1	114.6	-11.7	-8.6
Camden Bay	2	224	19.2	15.2	72.6	18.3	15.6	72.6	-7	3.8
Smith Bay	2	77	29.5	28.5	101	29	28.8	101	-22.4	5.3
MEAN	**2**	**1482**	**32.9**	**24.5**	**119.5**	**31.6**	**25.3**	**119.5**	**-7.8**	**4.2**
Argo	4	318	58.1	44.0	250.2	53.5	45.8	250.2	-16.0	4.5
Dinkum	4	541	65.9	46.7	235.5	60.5	49.4	235.5	-16.0	14.5
McClure	4	232	51.0	40.5	196.0	46.6	42.5	196.0	-0.2	8.3
Reindeer	4	90	75.5	53.9	170.4	72.2	54.5	170.4	-23.6	-16.7
Camden Bay	4	222	33.8	26.9	117.8	31.1	27.8	117.8	-14.3	8.0
Smith Bay	4	77	56.3	54.3	199.0	55.6	54.7	199.0	-44.9	10.8
MEAN	**4**	**1480**	**57.2**	**43.0**	**209.0**	**52.9**	**44.9**	**209.0**	**-15.2**	**8.3**
Argo	8	318	96.6	75.4	437.4	86	78.4	437.4	-30.5	8.6
Dinkum	8	541	110.7	79.2	398.5	100.6	82.5	398.5	-32.3	29
McClure	8	232	85.5	72.2	339.2	77.7	74.1	339.2	0.8	15
Reindeer	8	90	112.5	77.7	291.2	102.8	77	290.1	-53	-33.1
Camden Bay	8	218	58.9	47.5	181.6	53.5	49.6	181.6	-29.6	17
Smith Bay	8	77	105.4	104.9	370.9	103.9	105.7	370.9	-89.7	21.3
MEAN	**8**	**1476**	**95.9**	**73.6**	**356.6**	**87.0**	**76.1**	**356.5**	**-30.5**	**16.4**
Argo	12	318	123.5	97.1	588.9	107.2	99.4	588.9	-41.1	11.7
Dinkum	12	541	145.8	103.1	522.7	130	106.3	522.7	-47	42.2
McClure	12	232	112.3	92.6	445.3	100	94.6	445.3	4	18.1
Reindeer	12	90	142.6	96.5	308.3	130.4	95	308.3	-80.2	-47.9
Camden Bay	12	214	79.5	68.8	281.1	71.3	72.2	281.1	-46.7	27.1
Smith Bay	12	77	151.3	150.3	515.6	148	152.2	515.6	-134.8	31.8
MEAN	**12**	**1472**	**126.2**	**96.7**	**473.6**	**112.2**	**99.2**	**473.6**	**-44.0**	**23.4**

This page intentionally left blank.

Table 3: Landfast Ice Period Summary Statistics

Mooring	Analysis Length (days)	N	Mean Maximum Displacement (km)	Maximum Displacement Standard Deviation (km)	Greatest Maximum Displacement (km)	Mean Final Displacement (km)	Mean Final Distance Standard Deviation (km)	Greatest Final Displacement (km)	Mean Final Zonal Displacement (km)	Mean Final Meridional Displacement (km)
Argo	2	760	5.3	3.5	20.7	4.9	3.7	20.7	-0.7	0.1
Dinkum	2	1252	4.9	2.9	17.8	4.6	3	17.8	-0.3	-0.4
McClure	2	509	3.9	2.4	12.9	3.7	2.6	12.9	-0.5	1
Reindeer	2	258	4.5	2.9	17.6	4.1	3	17.6	-1.4	-0.5
Camden Bay	2	492	2.4	2.7	23.5	2.3	2.7	23.5	-0.3	-0.6
Smith Bay	2	249	2.7	1.7	12.3	2.6	1.7	12.3	-0.8	-1.2
MEAN	**2**	**3520**	**4.3**	**2.8**	**18.1**	**4.0**	**3.0**	**18.1**	**-0.5**	**-0.2**
Argo	4	750	9.2	6.0	35.6	8.2	6.3	35.6	-1.4	0.1
Dinkum	4	1242	8.5	4.8	34.1	7.6	5.1	34.1	-0.5	-0.8
McClure	4	505	6.9	4.4	23.7	6.3	4.6	23.7	-1.0	2.1
Reindeer	4	256	7.5	4.5	23.1	6.7	4.7	23.1	-2.8	-1.1
Camden Bay	4	488	4.4	4.7	30.9	4.3	4.8	30.9	-0.6	-1.2
Smith Bay	4	247	4.9	2.5	16.0	4.7	2.5	16.0	-1.6	-2.4
MEAN	**4**	**3488**	**7.5**	**4.8**	**30.4**	**6.8**	**5.0**	**30.4**	**-1.0**	**-0.4**
Argo	8	730	15.8	10.2	43.8	14.1	10.7	43.8	-3.0	0.3
Dinkum	8	1222	14.5	8.0	44.1	13.0	8.6	44.1	-1.1	-1.7
McClure	8	497	12.4	7.6	35.7	11.6	8.0	35.7	-2.1	4.2
Reindeer	8	252	12.6	6.8	34.9	11.2	7.1	34.9	-5.9	-2.3
Camden Bay	8	480	8.2	8.3	48.8	7.9	8.3	48.8	-1.3	-2.5
Smith Bay	8	243	8.8	4.0	18.5	8.5	4.2	18.5	-3.4	-4.8
MEAN	**8**	**3424**	**13.0**	**8.1**	**41.0**	**11.9**	**8.5**	**41.0**	**-2.2**	**-0.8**
Argo	12	710	21.6	14.4	62.8	19.3	15.1	62.8	-4.6	0.4
Dinkum	12	1202	19.9	11.0	61.6	17.7	11.8	61.6	-1.8	-2.6
McClure	12	489	17.6	10.8	48.6	16.6	11.3	48.6	-3.4	6.5
Reindeer	12	248	16.8	8.6	41.9	14.5	8.8	41.9	-9.0	-3.6
Camden Bay	12	472	11.7	11.7	75.5	11.4	11.7	75.5	-2.1	-3.7
Smith Bay	12	239	12.5	5.3	25.3	12.2	5.5	25.3	-5.2	-7.4
MEAN	**12**	**3360**	**18.0**	**11.2**	**57.9**	**16.4**	**11.7**	**57.9**	**-3.4**	**-1.2**

This page intentionally left blank.

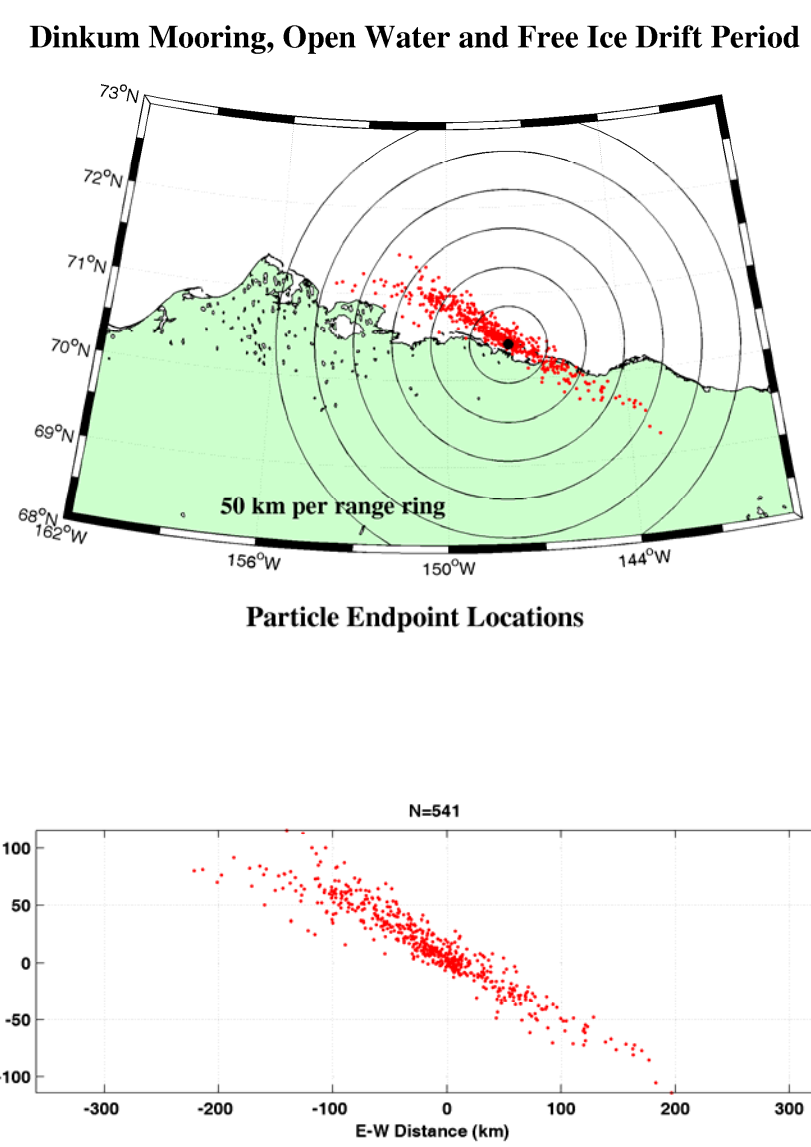

Figure 8. Particle endpoint locations (red dots) for all PVD iterations graphed on a map (upper panel) and in Cartesian space (lower panel) during the ***open water and free ice drift period***. The number N indicates the number days in the analysis. Particles were released once per day at the mooring site and were allowed to run for 4 days. The black dot locates the mooring position on the maps; the mooring is situated at (0, 0) on the lower panel. Particle endpoints that occur on land violate our assumption of spatial homogeneity and indicate a beaching would have occured. Range rings provide distance references from the mooring site. See **Table 1** and **Table 2** for additional details. These plots show that the flow is predominantly in the along-shore direction.

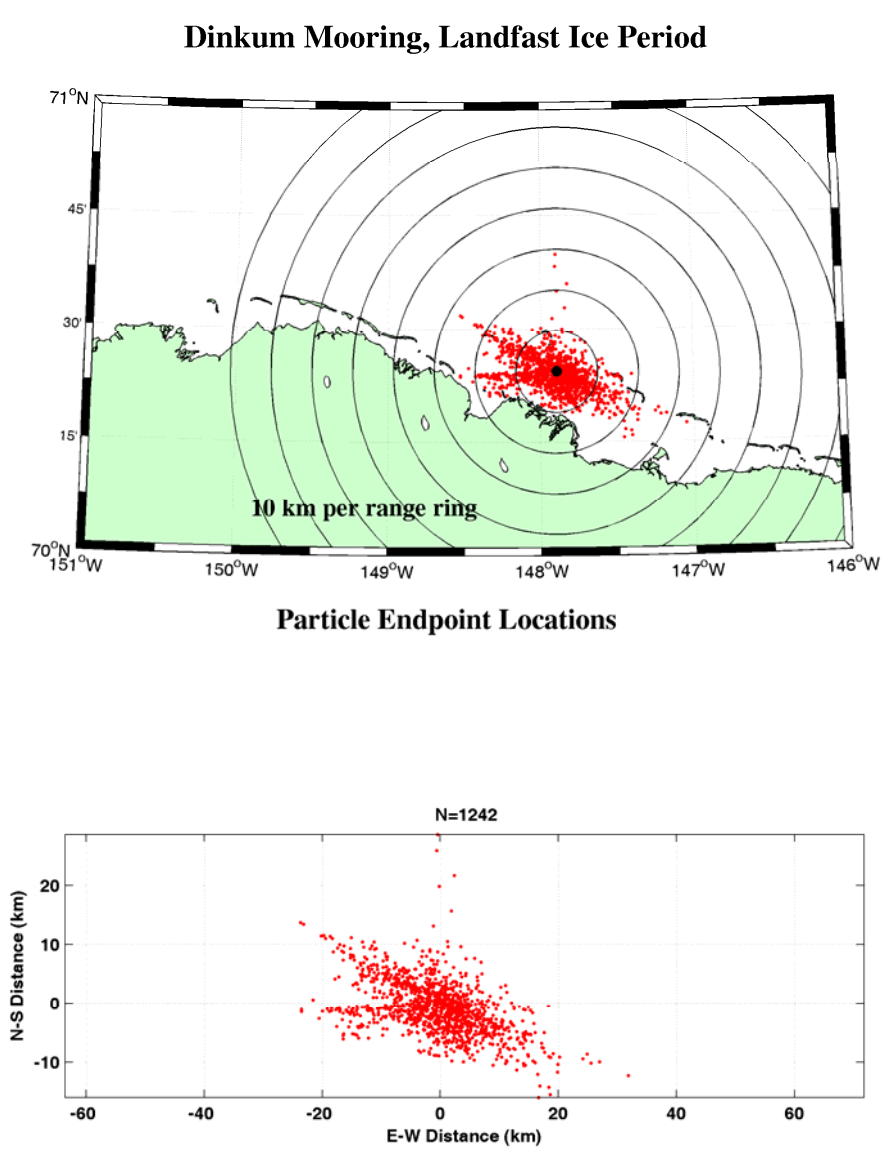

Figure 9. Particle endpoint locations (red dots) for all PVD iterations graphed on a map (upper panel) and in Cartesian space (lower panel) during the ***open water and free ice drift period***. The number N indicates the number days in the analysis. Particles were released once per day at the mooring site and were allowed to run for 4 days. The black dot locates the mooring position on the maps; the mooring is situated at (0, 0) on the lower panel. Particle endpoints that occur on land violate our assumption of spatial homogeneity and indicate a beaching would have occured. Range rings provide distance references from the mooring site. See **Table 1** and **Table 3** for additional details.

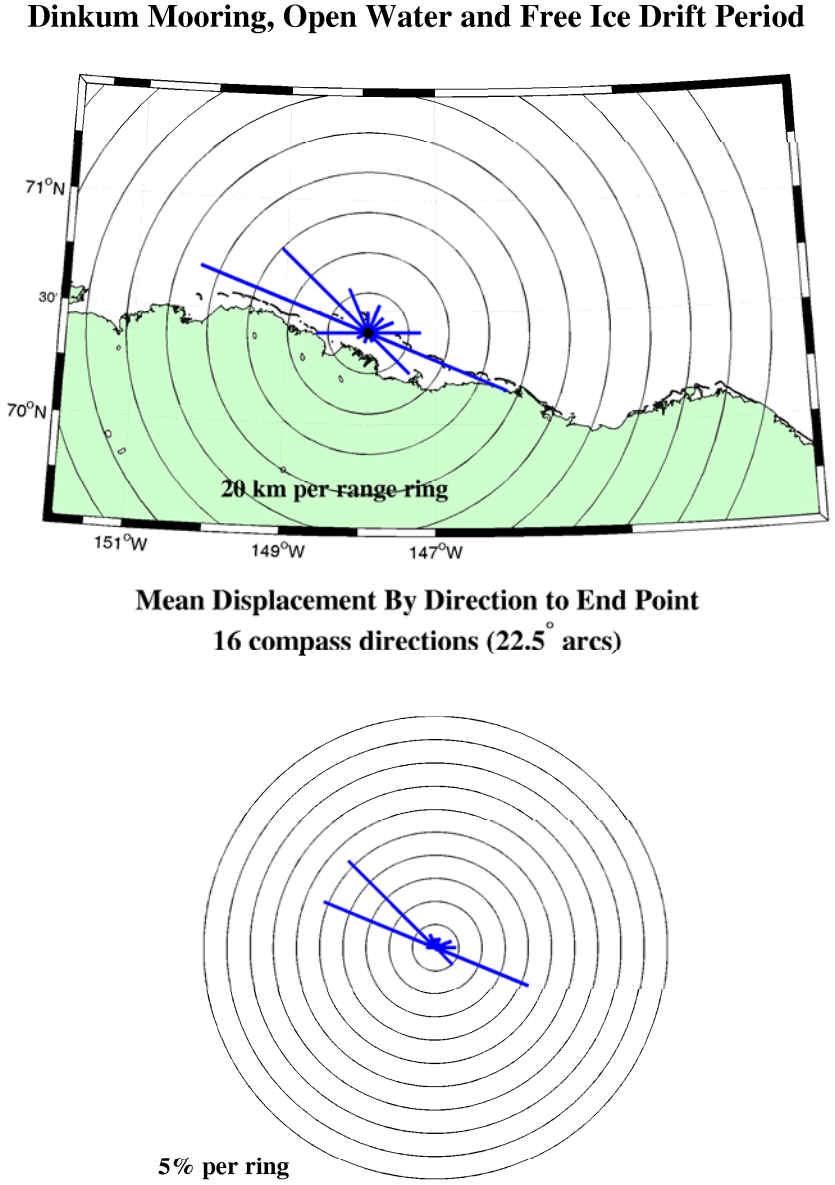

Figure 10. Average particle displacement based on the direction from the mooring to the particle end location (upper panel). The plots describe the mean PVD endpoint locations of all 4 day iterations (initialized daily) from the ***open water and free ice drift period***. Directions have been binned to 16 compass directions (22.5º arcs). For example, for bars indicating northward motion, we consider all endpoint located in the 22.5º arc spanning compass directions from 348.75º to 11.25º. The lower panel indicates the fraction of all particles that went in each of the 16 directions, given in percentage of the total. Each ring represents 5% of the total number of particles released. West is to the left, north to the top of the page. See also **Table 1** and **Table 2**.

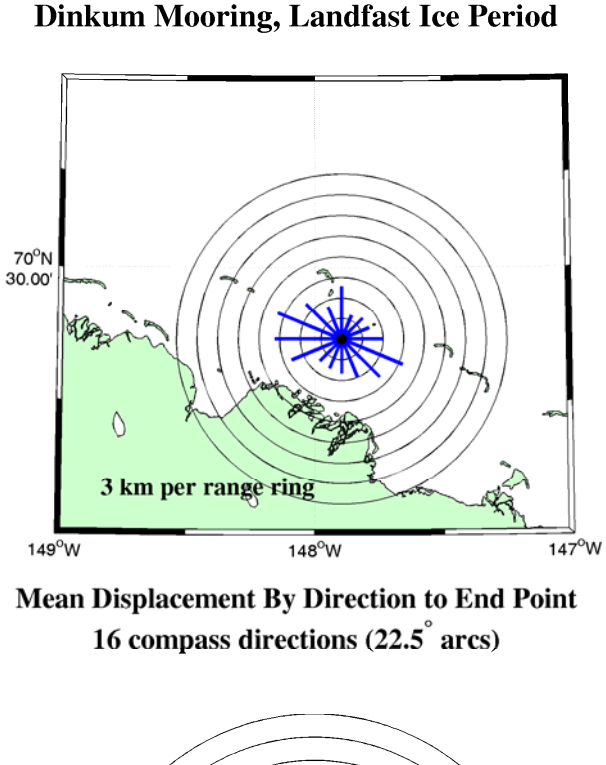

Figure 11. Average particle displacement based on the direction from the mooring to the particle end location (upper panel). The plots describe the mean PVD endpoint locations of all 4 day iterations (initialized daily) from the ***landfast ice period***. Directions have been binned to 16 compass directions (22.5º arcs). For example, for bars indicating northward motion, we consider all endpoint located in the 22.5º arc spanning compass directions from 348.75º to 11.25º. The lower panel indicates the fraction of all particles that went in each of the 16 directions, given in percentage of the total. Each ring represents 5% of the total number of particles released. West is to the left, north to the top of the page. See also **Table 1** and **Table 3**.

Dinkum Mooring

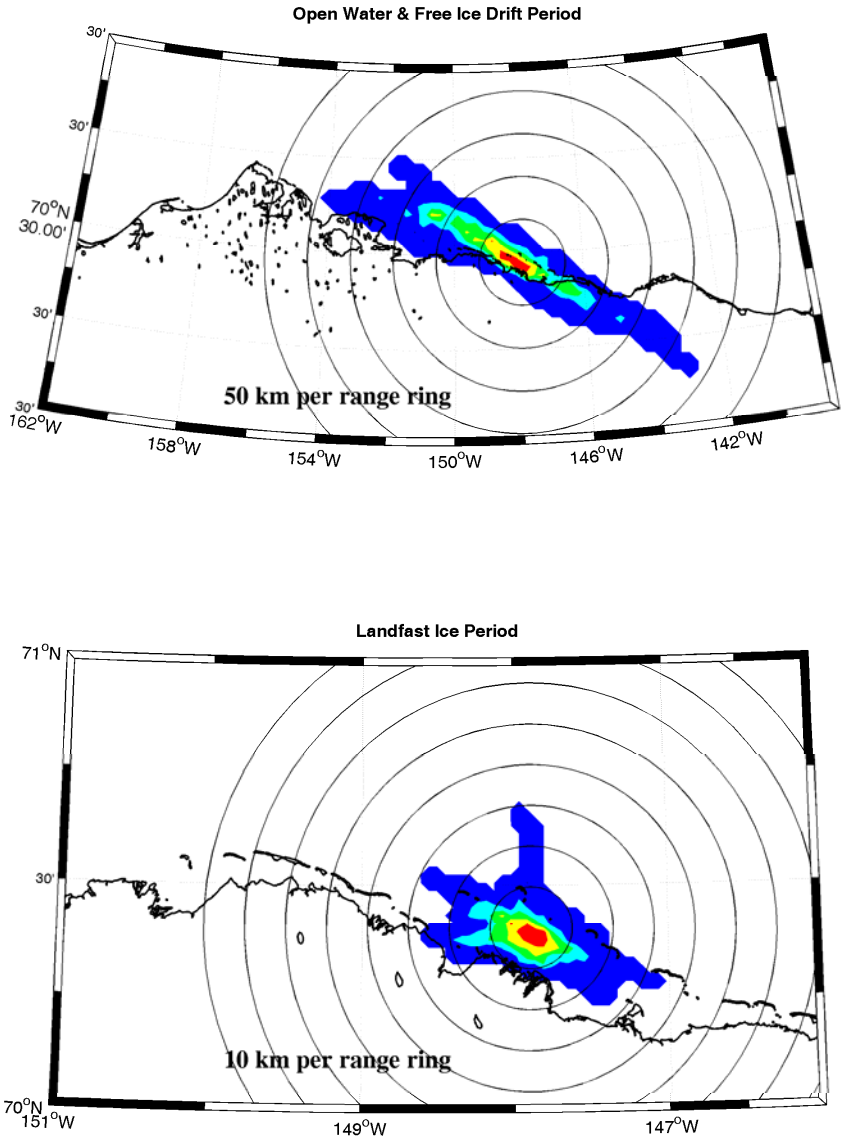

4-Day Analysis

Figure 12. Particle dispersion extent and density. The red areas have the highest density of particle endpoints, blue areas have the lowest endpoint density. Colors change at 20% increments. No particles were found in the white regions. 20% of all particle endpoint locations fall within the red area and the remaining 80% of all particles are found within the dark blue, cyan, green and yellow areas. Conversely, 80% of all particle endpoints fall within the cyan, green, yellow and red areas, with the remaining 20% in the dark blue area. To reduce noise, the PVD analysis was re-run for these plots with one analysis begun each *hour*, rather than once per day. Plots that depict gappy distributions (typically summer plots with only 1 or 2 years worth of data and long integration periods)

do not have enough data to adequately describe the likely distribution extent or probabilities for any particular area.

Plots with well-defined, non-gappy contours can serve as a useful design guide for oil spill response teams. For instance, if ADEC decides to incorporate an oil spill response plan that 1) would contain 80% of all oil spill events, 2) and can be mobilized within 4 days, the above plots indicate that the oil spill response team would have to be able to contain the spill within a 20 km alongshore distance and 10 km cross-shore distance during the winter, and within a 150 km alongshore distance, 25 km cross-shore distance during the summer.

6. Assessing oceanographic conditions during an oil spill

Familiarity with the modern suite of standard oceanographic sampling equipment will help ADEC assess the best available technology (BAT) for use in oil spill response efforts and general monitoring tasks. Recent advances in our ability to collect real-time data (from even subsurface instrumentation) allow us to collect timely oceanographic data from nearly any type of instrumentation package. We outline here some methods ADEC could employ during a spill response and ways that ADEC could prepare itself in order to conduct an efficient spill response.

A. Real-time monitoring of currents near offshore oil production activities

Summary statistical charts can aid in planning efforts, but actual conditions during a real oil spill event will unfold in a synoptic fashion. Real-time monitoring of currents in the Prudhoe Bay region would give responders the most accurate and timely information possible and would result in a more focused spill response effort.

A permanent ocean current monitoring station should be set up near oil production activities to provide real-time circulation data. A second-best option would be to assemble a stand-by ocean current monitoring system that could be rapidly deployed in the event of an oil spill. This would have the benefit of providing data as recovery efforts are underway; however this approach would miss data from the (possibly critical) initial days of a spill. Our measurements indicate that only one monitoring station can serve to describe nearshore currents within at least a 30 km radius during the winter months and over 100km in the summer months. Access to data that describe actual circulation conditions would allow oil spill cleanup efforts to be directed in an optimal fashion.

The technology for conducting real-time oceanographic monitoring is mature; however ice (in both summer and winter) presents special constraints on system design. For example, ice may preclude the use of direct cables to shore or surface buoys. Instead, underwater acoustic modems can transmit data from bottom mounted instruments. A seasonal deployment set up on landfast ice for the winter period (looking downward from the surface) can be set up to transmit data back to an operations center.

B. Data products provided by the Alaska Ocean Observing System

We recommend that ADEC personnel become familiar with the data products available at the Alaska Ocean Observing System (AOOS) web page (www .aoos.org). The AOOS group has taken the responsibility for collecting and disseminating oceanographic and atmospheric data related to Alaska's waters. Products include ocean temperatures, ice concentration, satellite imagery, wind conditions, and wind, wave and vessel icing forecasts. AOOS is also developing ocean circulation forecasts, though they are not yet operational (as of 2007). Given the sheer size and complexity of Alaska's waters, this fledgling effort will take some years to achieve full functionality. Support of their mission by ADEC would help ensure both the continued development of AOOS and

the enhancement of products they can deliver to emergency responders. AOOS welcomes feedback and suggestions about data products from all user groups and stakeholders, including agencies.

C. Other modern oceanographic sampling techniques

1. Surface current mapping

Current speed and direction data can be collected with ADCPs in real time at a single point, providing a profile throughout the water column. In the summer open water conditions, ocean surface current mapping high-frequency radars (HFRs) can collect hourly maps of sea surface velocity vectors. Example current vector maps from an HFR installation in Prudhoe Bay are shown in **Figure 13**. HFR data is increasingly being used by the US Coast Guard and other emergency responders around the country for purposes of search and rescue and other efforts that require knowing the speed and direction of surface currents.

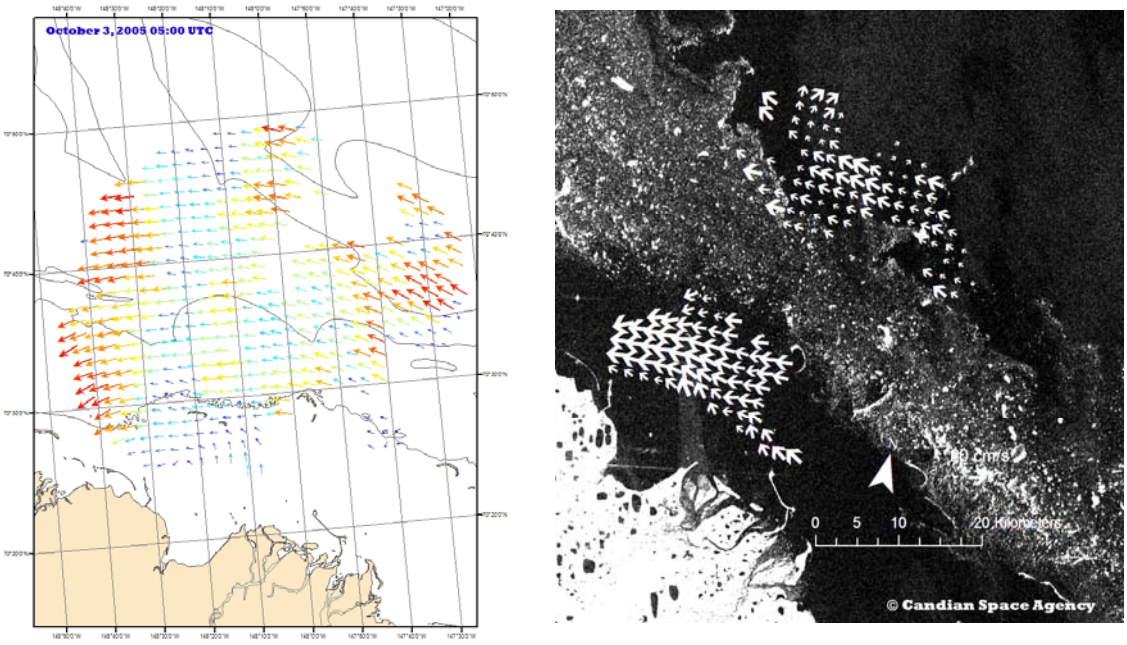

Figure 13. Two example depictions of surface current vectors from an HFR installation at Prudhoe Bay. The left hand map shows the typical spatial coverage and measurement density from a 12-13 MHz HFR installation. The vectors show inhomogeneity in the both the speed and direction of the surface current fields. Maps similar to these are generated on an hourly basis, processed and uploaded for internet access in real time. The image on the right shows current vectors superimposed upon a Synthetic Aperture Radar (SAR) image. This figure shows that currents are not resolved in regions of high concentration sea ice floes, which extend from the upper left to the lower right of the image. Additional details of HFR installations in both Cook Inlet and Prudhoe Bay are provided at: http://www.ims.uaf.edu/salmon/research/hf_radar/index.html. SAR image (c) 2006 Canadian Space Agency.

2. Oceanographic drifters

Transmitting position sensors with GPS accuracy can be left on floating sea ice and oceanographic drifters can be deployed directly into the water. Oceanographic drifters are carried by surface currents, transmit location data hourly, and can be used to track ice motion, water motion or oil slick motion. **Figure 15** shows a surface-following drifter and a sample trajectory diagram.

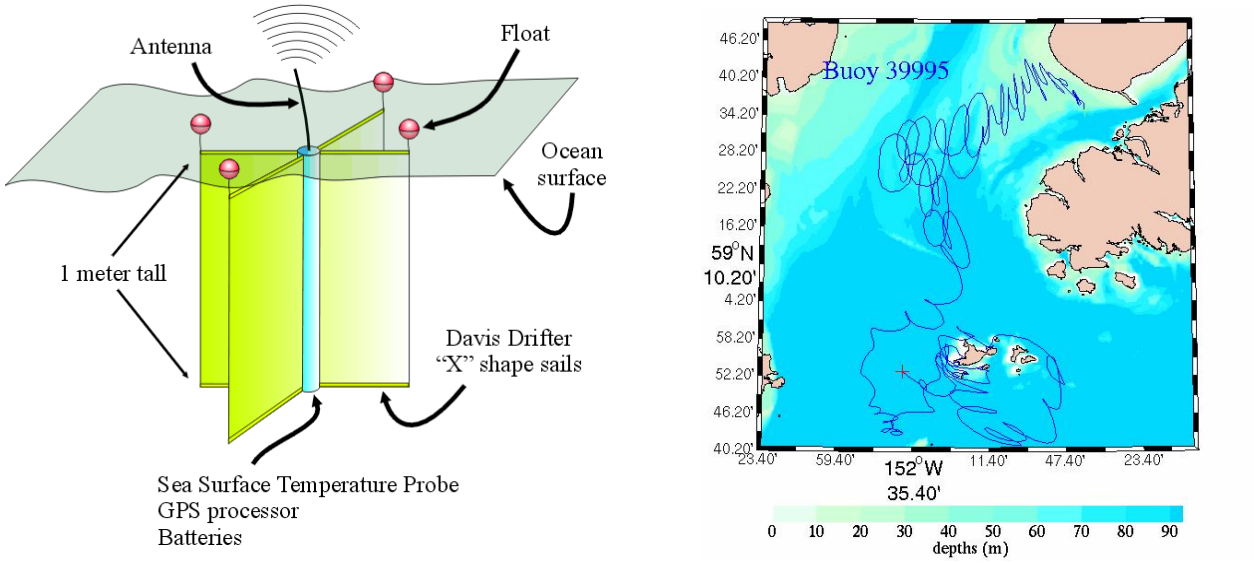

Figure 15. Diagram of an oceanographic surface drifter (left). Trackline of a drifter deployed in lower Cook Inlet in 2003 (right). Trackline courtesy of Dr. Mark Johnson; for details, see: http://www.ims.uaf.edu/research/johnson/cmi/.

3. New applications of technology: sensing oil beneath ice

In the event of an oil spill beneath the Alaskan landfast ice, aerial mapping of the spill extent is not currently feasible. To determine the spill extent would require a helicopter to land at a site along some transect, drill a hole in the sea ice, look for oil, then continue to a new test-hole site. The team would have to repeat this process along multiple transects to form a 2-dimensional grid in order to create a map of oil extent. This mapping method is inefficient and does not provide timely data. Each site would have to be re-occupied on possibly a daily basis to check its' status and the daily mapping operation would be dependent upon acceptable weather conditions. Snow machine transects towing a Ground Penetrating Radar (GPR) electronics package [Dickins, et al, 2006], could map oil extent under ice, though this method would be difficult to employ in heavily ridged areas. As with the helicopter transects, GPR oil mapping requires repeated transects to resolve the oil extent progression through time.

We believe that an oil spill response team would benefit from a network of small monitoring packages capable of sensing the presence of oil and telemetering the

information back to an operations base station. Oceanographers routinely make measurements with such electronic packages. Many fluorometers, normally designed to detect the presence of oceanic phytoplankton, can also detect the presence of oil. This behavior is due to oil's chemical properties that generate fluorescence when subjected to light at an appropriate frequency. Applying this technology would be novel in ice covered waters for the purpose of oil spill response but we see no reason it would not be a practical and valuable tool for a response team. Such a device would improve field logistics, personnel safety and timeliness of decision making during an actual spill response effort.

We envision a small package that could be left at each hole and could "look" for the presence of oil. This package could transmit its data to a response center several times per hour. With a network of tens or hundreds of such devices, responders could create a detailed picture of the oil spill extent in real time. The PVD maps presented in this report would help guide a deployment strategy for these packages. Similar packages could be deployed as monitoring devices at critical offshore locations, for example, along a pipeline or near production activities. A modest pilot study could test the feasibility, design and operation of such a monitoring device network.

4. Autonomous underwater vehicles and remotely operated vehicles

Unmanned underwater missions can be carried out by Autonomous Underwater Vehicles (AUVs) and Remotely Operated Vehicles (ROVs), which incorporate video, sidescan sonar and other imaging tools in addition to standard oceanographic instrumentation. AUVs can presently carry out unattended daylong missions; within the next decade, 6-month deployment capabilities will be realized. AUVs can be employed to visually inspect underwater cabling or oil pipeline routes. They could also survey the ice underside with video cameras to look for pools of oil during a spill. **Figure 14** shows a commercially available AUV. ROVs remain attached to the surface by an umbilical power and communications tether. They can dive to depths deeper than the AUVs and are commonly used in recovery, underwater construction, videography, and cable trenching operations. The tether limits their under-ice use to applications relatively close to the deployment hole, but ROVs have the advantages of being transmit real time data and can accommodate large payloads.

Figure 14. The Hugin AUV, manufactured by Kongsberg Maritime. This AUV has an endurance of up to one day, can dive to 1000 m depths and can travel at over 4 knots.

7. Recommendations for future study

From the oceanographic perspective, additional efforts could further enhance ADEC's ability to effectively respond to oil spills during both the summer and winter seasons. Each season presents its own set of challenges to effectively contain an oil spill. In the winter, inclement weather conditions can inhibit safe and timely access to a spill site and pores in the ice can trap oil, only to be carried away after breakup. Simply mapping the spatial extent of an oil plume in winter will pose a logistical challenge. In the summer, wind-driven currents can displace an oil slick great distances very quickly.

In Section 6, we described technology that ADEC could employ to better assess oceanographic conditions and oil extent during an oil spill response. Below, we outline a number of efforts that would increase our understanding of the oceanographic circulation in the Beaufort Sea, efforts that would also lead to a more fully informed oil spill response. They range in scope from modest and relatively straightforward analyses of existing datasets to extensive field experiments.

A. Synthesis of existing data sets

1. Combined analysis of the ADCP records with other data

The current meter measurements described here provide a picture of oceanographic conditions as viewed from 6 individual locations. Other datasets could be analyzed in conjunction with these velocity measurements to construct a more complete view of the system. Such analyses would help quantify the spatial extent of the domain for which these analyses are valid. Examples of existing complimentary data sets include the following: weather station or atmospheric model wind and atmospheric pressure records, satellite-based wind speed measurements over open water and 2-dimensional mapped ocean surface current measurements (HFR).

2. Model verification

Our velocity, pressure, temperature and salinity datasets present the best opportunity to date for verification of circulation models in the nearshore Beaufort Sea. High resolution numerical models of oceanic circulation are capable of estimating wind-driven, tidal and buoyancy-forced flows. Many oil spill trajectory models are based upon wind-driven circulation only; the influence of landfast ice in the Beaufort Sea renders such simple models ineffective. In addition, parameterization of frictional coupling between the ice, currents, atmosphere and wind are approximate at best and render model predictions suspect without proper verification. Coupled atmospheric-ice-ocean models exist for the Beaufort Sea but have not been thoroughly verified nor compared to observational data in any rigorous fashion. Such comparisons would help provide a proper framework for interpreting model results.

B. Oceanographic field studies

1. Measurements distributed across the shelf

Having only recently gained the ability to collect year-round oceanographic data in the near shore Beaufort Sea, our database is still small, confined close to shore and lacks coverage near major river deltas. Deployment of moorings in the cross-shelf direction remains a major task for the future and is needed to help quantify exchange between the nearshore and offshore regions. Such deployments may be riskier due to ice keels scouring the bottom beyond the landfast ice zone but are essential to accomplish for a complete understanding of the Beaufort circulation.

2. Measurements near river deltas

While we have made one partially successful deployment in Smith Bay (the mooring was destroyed by ice after 11 months, but most data nonetheless recovered), we have no year-round oceanographic moorings between our Reindeer and Smith Bay sites. We expect that oceanographic conditions near Harrison Bay to be different than those near Prudhoe Bay because of the large river discharges from the Colville and Kuparuk rivers. Such conditions could affect interpretation of the results given in this report (particularly during the summer months). We still lack the oceanographic measurements that would apply to an oil spill in the Harrison Bay region.

3. Resolving the under-ice topography

Lack of detailed knowledge of the under-ice topography limits the ability of numerical models and analytical solutions to evaluate and predict ocean circulation. High quality 2-dimensional mapping of the ice underside across the landfast, transition and pack ice zones in the Beaufort Sea would be a major step forward for a number of disciplines, from ice dynamics to ocean circulation modeling. Without such measurements, oil spill trajectory models for the Beaufort Sea will not be able to accurately predict the fate of a winter oil spill. Aircraft-based electromagnetic (EM) ice topography measurements could be an important part of an on-scene oil spill response, by being able to map a large area quickly. Airborne EM sensors can measure ice thickness at an accuracy of 0.1 m with a horizontal footprint of 20-40m, depending on the helicopter flight altitude. The most accurate topographic sampling (though slower) would be done with an AUV survey or with a snowmachine-based EM survey.

4. Measurement of currents within and through the surface stratified layer

A field study designed to profile the entire water column currents up to the underside of the ice, particularly during the spring freshet, would help us describe the upper layer shear and quantify the surface currents currently not resolved by the ADCP measurements. HFR will do a good job in late August and September, but through-ice studies are required in June and July. The fate of the fresh spring plume has ramifications for cross-shelf exchange of fresh water, sediment and oil.

8. Summary

The analyses presented here comprise our best estimate of particle displacements over short time periods based upon in-situ oceanographic data from the nearshore Alaskan Beaufort Sea. With enough data, the statistical properties of these ensembles will describe probable bounds for oceanic dispersal of freely drifting oil over the integration time frame. The accuracy of the PVD analyses degrades with distance from the mooring site and with the length of the integration. The value in our results lies primarily in our ability to place approximate bounds on the length scales over which we might expect oceanic advection to play a role for a given time period.

Primary findings include the following. 1) Over the 2-day to 12-day time frames considered here, displacement of an oil spill will be relatively small during the landfast ice period (tens of kilometers) and relatively large during the open water and drifting ice period (hundreds of kilometers). 2) Transport in the summer is highly dependent upon the wind speed and direction. 3) In both seasons, transport of oil in the alongshore (east-west) direction is greater than transport in the cross-shore (north-south) direction.

We find that over a 12 day period, an oil spill at our mooring locations during the landfast ice period would *on average* be confined to within 18 km of the spill site. In contrast, over the same period of time during the summer, the primarily wind-driven flow would transport an oil spill *on average* a distance of 126 km. Over a 4 day period, the average oil spill extent for the two seasons is 8 km and 57 km respectively.

In aggregate, the findings suggest that the average oil slick leading edge would move 1.5-2 km per day in the winter and 10-15 km per day in the summer. In rare cases, oil could move 6 km/day in the winter and 60 km/day in the summer. In general, frictional coupling, trapping of oil in ice pores, topographic steering, or other interactions between the oil, water and ice will degrade the accuracy of the results. However, due to lack of detailed knowledge about the under-ice topography and the coupling between ocean currents, crude oil and actual sea ice; it is not possible in this report to quantify the uncertainty of our estimates.

The length scales resolved by these analyses can help emergency responders know how much time they might expect to have to contain an oil spill within a given radius at a given site. The most robust bounds come from the landfast ice period at multiyear deployment locations. For moorings with only one year's worth of data, the total number of summer integrations is small and the resulting ensemble of integrations may not be a statistically representative depiction of all possible particle displacements for the summer season. Nonetheless, it is clear that the summer analyses indicate possible displacements of great distances (>200km) over time periods of less than 12 days and that the summer circulation is strongly dependent upon the winds.

The figures and tables included within this report can help ADEC design a response plan based on arbitrary containment thresholds. For example, ADEC may strive for the ability to mobilize a response within 4 days of a spill event near the Dinkum site

and that the response should be able to contain the leading edge of at least 80% of all spill events. Based on **Figure 15**, this scenario requires that ADEC be prepared to contain the spill within a ~100km radius in the summer and within a10 km radius in the winter. If the objective is to contain an oil spill before oiling of beach occurs, the tables and figures in this report can help guide the appropriate response guidelines for a particular location. **Figure 12** can be used to estimate the along-shore vs. cross-shore distance a response must cover based on the density of endpoint locations.

Knowing the in-situ wind speed and direction in the summer (**Figure 3)** will provide a good measure of the actual direction and distance the oil spill would travel. Real-time monitoring of ocean currents is presently the only way to determine which direction the spill would tend to spread in the winter.

ADEC can improve its oil spill response preparedness for the Beaufort Sea by investing in three types of effort. First, analysis of existing datasets and model outputs in conjunction with the velocity data analyzed here would help place the results of this report in a broader spatial context. Second, much basic oceanographic research is still needed to understand the nature and causes of circulation over the Beaufort shelf and it spatial variability. Third, implementing an oceanic monitoring program for the purposes of knowing ocean conditions before and during an oil spill would allow spill responders to act in a more fully informed fashion and make better decisions. New technologies can be employed to efficiently aid in an actual oil spill response effort.

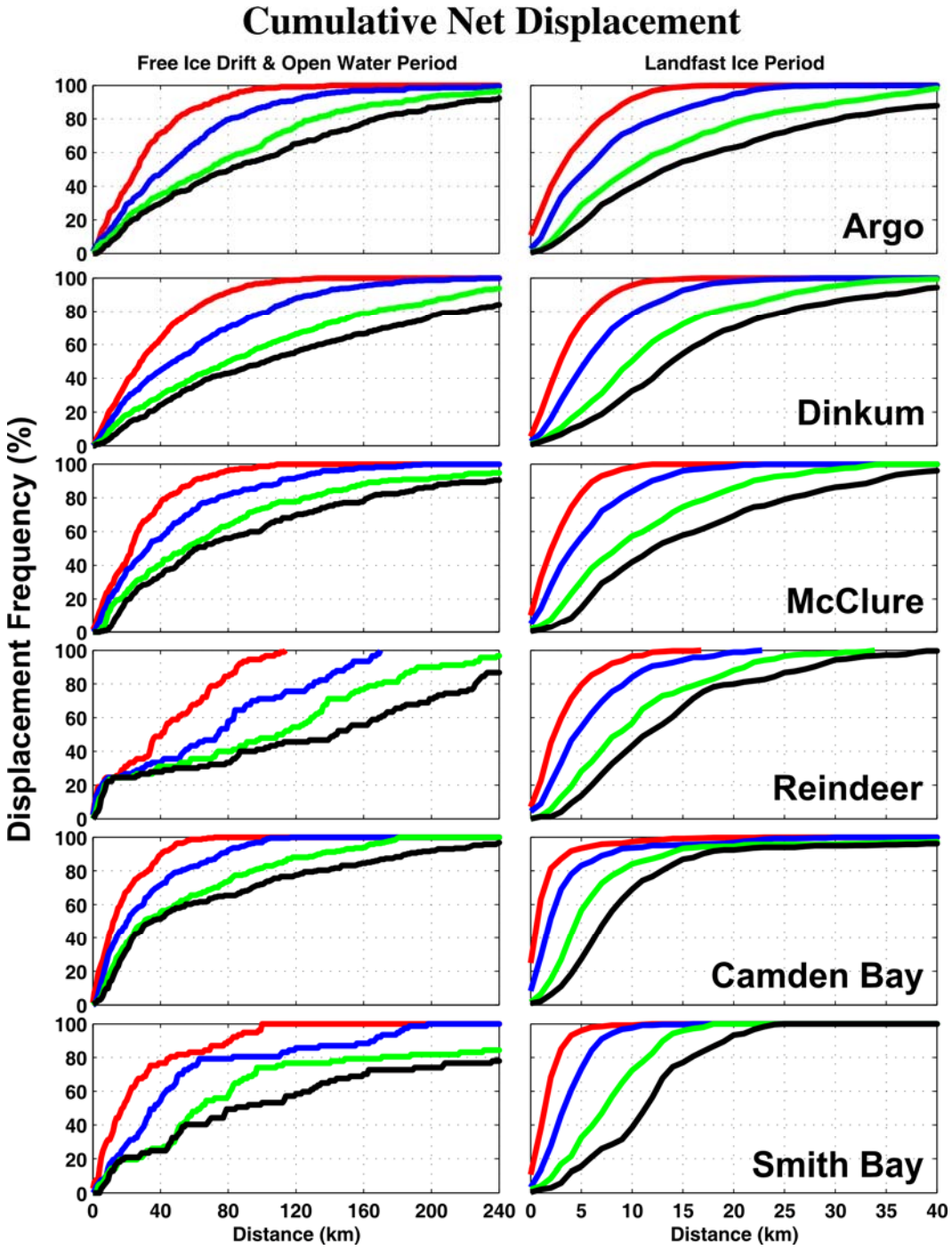

Figure 15. Cumulative displacement frequency at all six mooring sites during the summer (left) and winter (right). Based on concentric circles centered about the mooring site with radii given by the distances on the horizontal axis, the vertical axis describes the fraction of all particle endpoint locations found within each circle. The colors red, blue, green and black are associated with the 2, 4, 8 and 12 day analyses, respectively. This plot can be used as an oil spill response planning tool as described in the accompanying text.

9. References

Aagaard, K., 1981, Current Measurements in Possible Dispersal Regions of the Beaufort Sea, OCSEAP final report A81-02, RU91, 74 pp.

Aagaard, K., C. H. Pease, A. T. Roach and S. A. Salo, 1989, Beaufort Sea Mesoscale Circulation Study; (in) Outer Continental Shelf Environmental Assessment Program, Final Reports of Principal Investigators 65:1-427 (NTIS PB90-124181/AS) RU 0686

Barnes, Rearic and Reimnitz, 1984, Ice gouging characteristics and processes, in The Alaskan Beaufort Sea: Ecosystems and Environment, ed. by P. W. Barnes, D. M. Schell, and E. Reimnitz, 185 - 212. Academic Press, New York

Cox, J. C. and I. A. Schultz, 1980, The transport and behavior of spilled oil under ice. Proceedings of the Third Annual Technical Seminar, Arctic Marine Oil Spill Program, Edmonton, June 1979, p. 45 – 61

Dickins, D., P. J. Brandvik, L. Faksness, J. Bradford and L. Liberty, 2006, 2006 Svalbard Experimental Spill to Study Spill Detection and Oil Behavior in Ice, Final Technical Report, Minerals Management Service, Contract 1435-01-06-CT-3925, 94 pp.

Gordon, R. L., 1996, Acoustic Doppler Current Profiler Principles of Operation – a Practical Primer, RD Instruments, San Diego, CA, 54 pp.

Mahoney, A., H. Eicken, L. Shapiro and A. Graves, 2005, Defining and locating the seaward landfast ice edge in northern Alaska**,** paper presented at the 18th International Conference on Port and Ocean Engineering under Arctic Conditions, POAC ‘05, Potsdam, N.Y., June 26-30, 2005, vol. 3, 991-1001.

Weingartner, T. J., S. R. Okkonen, and S. L. Danielson, 2005, Final Report: Circulation and Water Property Variations in the Nearshore Alaskan Beaufort Sea prepared for MMS, Contract 1435-01-00-CA-31083, 103 pp.